An alternative experimental configuration to generate wrench zone above a viscous layer

B. C. Vendeville, G. Corti, M. Boussarsar, O. Ferrer

Journal of Structural Geology 184 (2024) 105166

Contents lists available at ScienceDirect

Journal of Structural Geology

journal homepage: www.elsevier.com/locate/jsg

An alternative experimental configuration to generate wrench zone above a viscous layer

B.C. Vendeville [a], G. Corti [b], M. Boussarsar [c], O. Ferrer [d,*]

[a] Université de Lille, CNRS, Univ. Littoral Côte D'Opale, UMR 8187, LOG, Laboratoire D'Océanologie et de Géosciences, F 59000, Lille, France
[b] Consiglio Nazionale Delle Ricerche, Istituto di Geoscienze e Georisorse, Via G. La Pira, 4, 50121, Florence, Italy
[c] Université de Sfax, Fac. Sciences de Sfax, Laboratoire GéoModèle - LR16ES17, BP 1171, Sfax, 3000, Tunisia
[d] Institut de Recerca Geomodels, Departament de Ciències de La Terra I de L'Oceà, Facultat de Ciències de La Terra, Universitat de Barcelona, 08028, Barcelona, Spain

ARTICLE INFO

Keywords:
Wrench zones
Strike-slip
Riedel experiments
Analogue modelling

ABSTRACT

Analogue modelling of wrench tectonics typically utilizes a rigid basement with a velocity discontinuity under a brittle or brittle-viscous cover, such as in Riedel experiments, which confines fault localization in the overlaying model. However, such a set-up is hardly compatible with modeling brittle-ductile systems such as the upper and lower crust or a brittle sedimentary cover overlying a viscous evaporitic layer. To achieve a more realistic experimental approach, Bruno Vendeville designed an alternative experimental set-up decoupling the basement from the brittle overburden with a viscous layer in which the basement is not involved. In this configuration, strike-slip movement is driven laterally rather than from the base up, facilitated by "weak zones" that preferentially localize the deformation during shortening and enable sliding between compartments. This original approach provides greater flexibility for modeling complex strike-slip settings, allowing for more freedom for strike-slip structures to form and evolve through time.

Although the experiments described in this work were conducted in the late 1990s, the co-authors have chosen to revisit and adapt this earlier work for this Special Issue to underscore Bruno's influence on another aspect of salt tectonics and his pioneering foresight in the field of analogue modelling.

1. Introduction

Wrench zones are some of the most challenging structures to simulate with physical (sandbox) models. In experiments involving pure extension or shortening, the structures form perpendicular to the direction of movement imposed by moving walls and terminate along-strike along the sidewalls (e.g., Fig. 7a in Ferrer et al. (2014) for pure extension models and Fig. 3a in Borderie et al. (2018) for pure shortening models). Hence the lateral conditions usually do not interfere much with the deformation pattern and the structural evolution, except for the potential effect of lateral friction along sidewalls. Instead, when modeling strike-slip zones one needs to consider the boundary conditions on all four sides, with deformation which is normally *ad-hoc* imposed by motion of rigid plates (Riedel experiments, see below) therefore limiting the freedom of structures to develop in a narrow linear system.

Nearly all the Riedel experimental set-ups dating from the pioneering works of Cloos (1928 and 1950), Riedel (1929), Cloos (1955), and Tchalenko (1970) (see also Naylor et al., 1986; Schreurs, 2003, and the extensive review by Dooley and Schreurs, 2012) have imposed the strike-slip movement from the base up using two adjoining rigid basal plates that slide one past each other along a velocity discontinuity (hereinafter VD) parallel to the imposed horizontal displacement (Fig. 1a). This VD simulates a pre-existing fault affecting the rigid basement, and the overlying layered sand pack representing the sedimentary cover that deforms with a brittle behavior resulting in a set of faults rooted at the VD and localized within a narrow belt in the immediate surroundings of the VD (red surfaces in Fig. 1b). The Riedel experimental set ups allowed to simulate the existence of a single or multiple basement faults (velocity discontinuities between basal plates) (e.g., Schellart and Nieuwland, 2003). Using a Riedel experimental set up, other studies have investigated the interaction between wrenching tectonics and crustal weak zones or pre-existing weak bodies such as magmatic intrusions, volcanic calderas, or diapirs (i.e., Corti et al., 2005; Román-Berdiel et al., 1997; Letouzey and Sherkati, 2004; Koyi et al., 2008; Dooley and Schreurs, 2012; Gomes et al., 2019).

* Corresponding author.
E-mail addresses: giacomo.corti@igg.cnr.it (G. Corti), boussarsar.marwa.geo@gmail.com (M. Boussarsar), joferrer@ub.edu (O. Ferrer).

https://doi.org/10.1016/j.jsg.2024.105166
Received 19 September 2023; Received in revised form 15 May 2024; Accepted 15 May 2024
Available online 17 May 2024

Unlike what is observed in Riedel experiments, where deformation is constrained within a narrow band above the VD, strike-slip related structures in nature tend to be distributed in broad zones (i.e., Dead Sea fault system - Girdler, 1990). To simulate more realistic structures, Mandl (1988) modified the Riedel experiment with a rubber sheet partly glued to both rigid base plates allowing a more distributed strike-slip deformation of the overlaying sand pack. Other experimental designs (Schreurs, 1997, 2003; Schreurs and Colleta, 1998), imposed regional wrenching by adding a set of plexiglass bars confined by wooden slats that, as the deformation progresses, allow them to move like a stack of cards by a system of pins fixed at the basal plate base and the lateral walls of the model (see Fig. 1 in Schreurs, 2003). The model is then built on top of a silicone layer overlying the plexiglass bars, simulating a basin-scale or a middle to lower crustal detachment, that allows a distributed deformation at the base of the model and in the overlaying sand (brittle-viscous model). In contrast to Riedel experiments with two basal plates and a VD, in this experimental set-up regional wrenching was imposed by the combined movement of the base and the lateral walls of the model (Schreurs, 2003). These second type of experiments are beyond the scope of our work, so we will primarily focus on the description of an original setup that is then compared with the Riedel-type experiments.

The overburden of Riedel experiments has been classically simulated with sand (i.e., Naylor et al., 1986; Richard et al., 1995 or Viola et al., 2004 among others) or wet clay (i.e., Tchalenko, 1970; Hatem et al., 2017 or Toeneboehn et al., 2018 among others) without a basal *décollement* (brittle models). Other authors used a basal viscous *décollement* of silicone overlaid by a sand pack (brittle-viscous model, i.e., Casas et al., 2001) or a combination of both (i.e., Rosas et al., 2014). The mechanical properties of the overburden materials impact directly on the final geometry of the resulting structures (see Dooley and Schreurs, 2012 for specific information), leading to the development of *en-échelon* Riedel shears or flower structures that systematically root at depth onto the VD (Fig. 1b) (i.e., Naylor et al., 1986).

However, when addressing wrench zones in different geological scenarios, such as faults affecting the upper continental crust or shallower faults in a sedimentary cover and rooted in a weak layer, such as evaporites or shales, the challenges become threefold.

1) Although the VD between the moving base plates may simulate specific natural cases in which deformation is controlled by reactivation of crustal or basement pre-existing structures (e.g., Zwaan et al., 2019), this experimental set-up may not reproduce other geological scenarios in which inherited structures are absent or play a negligible role on strike-slip deformation.
2) The brittle layer is underlain by a viscous material (whether the lower crust or evaporites) that has almost always a mechanical strength much lower than that of the overlying brittle layer (Fig. 2).

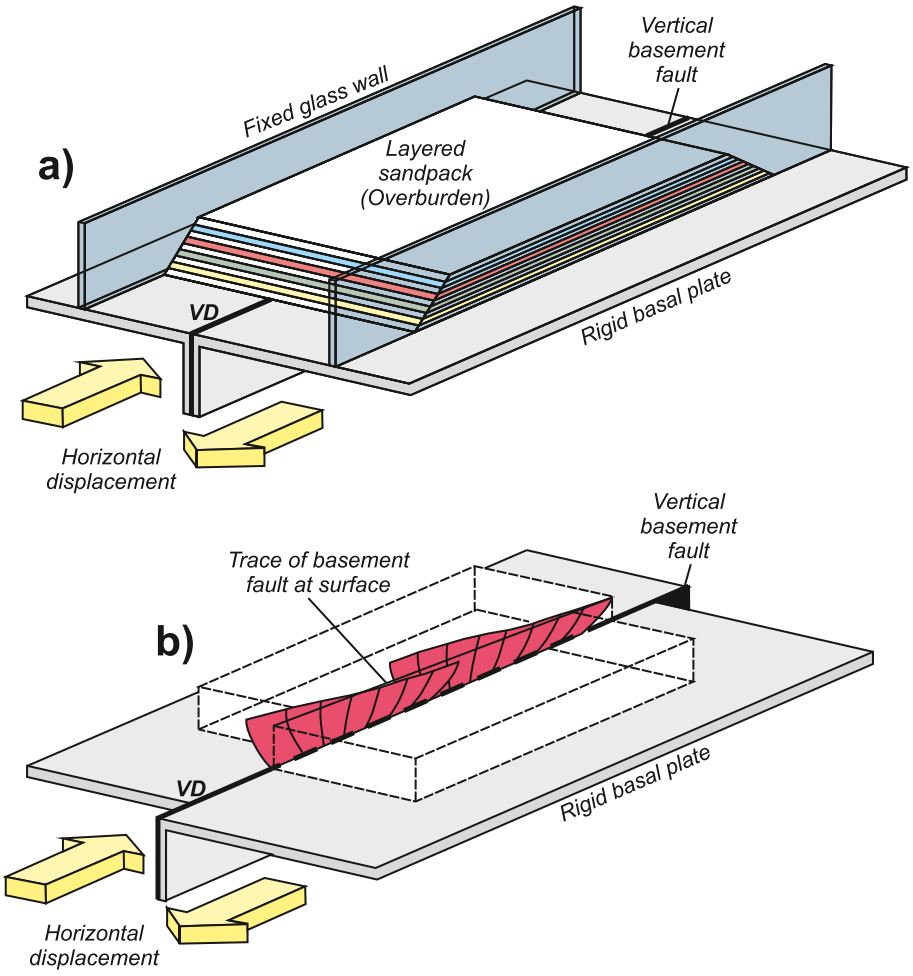

Fig. 1. a) Simplified sketch of the classical Riedel experimental set-up (Tchalenko, 1970) using two rigid basal plates (grey) beneath the layered sand to simulate wrench faults. The boundary between both basal plates (VD) simulates a vertical basement fault and the overlying layered sandpack the brittle overburden. **b)** Schematic 3D geometry of Riedel shears (reddish surfaces) resulting from the relative dextral displacement of the basal rigid plates of the previous set-up. Modified from Naylor et al. (1986).

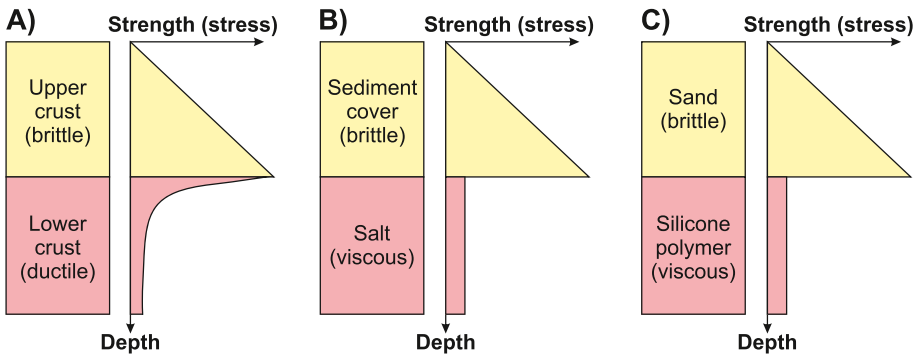

Fig. 2. Schematic strength profiles **A)** for the continental crust, B) a sedimentary cover overlying a viscous layer, and **C)** a sand/silicone model. The curves indicate the stress value. The areas indicate the strength in terms of forces.

3) Using a rigid basement imposes the localization of the structure during their formation and their following growth, leaving little or no leeway for their own evolution.

Here, we present an alternative experimental set-up to the classical Riedel experiment (Cloos, 1928; Riedel, 1929) by avoiding the use of rigid basal plates. In addition, this alternative set-up also allows, with some modifications, to successfully study the deformation of pull-apart basins without the classical rigid basal metal plates or pre-existing discontinuities (i.e., Boussarsar et al., 2022; Peng et al., 2024). While the experiments included in this work were conducted in the late 1990's by the first author, the co-authors have decided to revive and revise this older article for the Special Issue. This decision aims to underscore Bruno's impact on another facet of analogue modelling, showcasing his foresight and pioneering contributions in the field.

2. An alternative DESIGN for triggering wrench zones without using basal discontinuities

The experimental set-up used in this study consists on a deformation box of 112 cm long and different widths depending on the models with two mobile end walls and two fixed lateral glass sidewalls (Fig. 3). The box includes a viscous, tabular basal silicone layer covering the entire model overlaid by a brittle layered pack of dry white and colored quartz sand layers without any pre-existing regional fabric or fault (Fig. 3). A regular grid of 1.5 × 1.5 cm carefully placed on the surface of the models allows to visually monitor progressive deformation and offsets along faults during the experiments. So far, this experimental set-up is a standard configuration for an extension or contraction model (i.e., Ferrer et al., 2014; Borderie et al., 2018 respectively). Two "weak zones" were created by locally vacuuming part of the brittle overburden during the construction of the model (Fig. 3). These "weak zones" were located

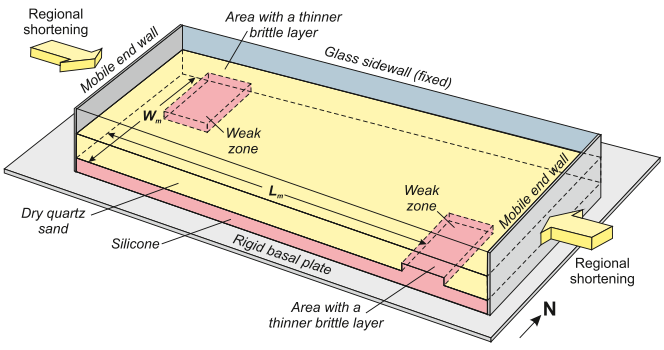

Fig. 3. 3D conceptual sketch illustrating the initial set-up of the models presented in this work. Note the north direction indicating the orientation framework of the model and the developing structures.

at two opposite corners of the model occupying half the width of it (pink polygons within the yellow overburden in Fig. 3). A motor-driven worm screw transferred the deformation to the sandbox by pushing the mobile end wall(s) towards the model's center, therefore shortening the models at a constant velocity of 5 mm/h (Fig. 3 and movie in supplementary material). The experimental program including the two models presented here was carried out with one or two movable end walls indistinctively without any significant differences between both procedures. In order to prove it, we present a model performed with one and two mobile walls (Model 2 and Model 1 respectively).

At crustal scale, the "weak zones" may be analogous to pre-existing basins reactivated during compression. An example of natural prototype could be the Palmyride foldbelt and the Taurus structure that located at the northern end of the Dead Sea strike-slip zone accumulate up to 105 km of strike-slip movement in the last 20 Ma (Ben-Avraham and Lyakhovsky, 1992). There, a pre-existing basin that was reactivated in compression as the Eurasian block moved northward with respect to the Arabian plate. Additionally, at smaller scale, the weak zones can simulate dormant diapirs, salt walls or salt sheets linked by tear faults under contraction (Rowan et al., 1999; Ferrer, 2012; Dooley et al., 2015; Duffy et al., 2021).

The models were built with materials typically used to simulate upper crustal deformation. Dry well-sorted quartz sand with an angle of internal friction 30-31°, a density of 1760 kg m^{-3}, and 300 mm grain size (Vendeville and Jackson, 1992) was used as a mechanical analogue of brittle rocks (Fig. 2c). Colored sand was dyed using organic and mineral pigments with no variations on the mechanical properties. For the construction of the layered overburden, sand was poured on the model and then levelled with a manual scraper. On the other hand, a transparent polymer (SGM-36 manufactured by Dow Corning) with a nearly-Newtonian behavior at the experimental strain rates was used as analog of ductile lower crust or viscous salt (Weijermars, 1986) (Fig. 2c). The density of the polymer is 970 kg m^{-3} and the dynamic shear viscosity measured by Vendeville and Jackson (1992) in a coaxial viscometer changes from $2.5x10^4$ to $3.3\ x10^4$ Pa s at a strain rate of $3x10^{-1}$ and $2\ x\ 10^{-3}\ s^{-1}$ respectively, at a room temperature of 23 °C. The silicone layer was built from different chunks leaving them between 24 and 36 h to flow and homogenize. The scaling ration between models and nature is around 10^{-5}, such that 1 cm in the models represents 1 km in nature (Hubbert, 1937; Ramberg, 1981).

The particularity of the experimental set-up presented in this work, unlike the one used in Riedel experiments where the strike-slip movement is imposed by the relative displacement of the two rigid basal plates along the velocity discontinuity (Riedel, 1929; Tchalenko, 1970), is that wrenching is triggered by lateral forces simulating regional shortening. Because the overall mechanical strength of a brittle-viscous system depends mostly on the brittle layer, the areas where this one is locally thinner (i.e., above the "weak zones") can deform much more easily compared with the rest of the model (Fig. 3). In other words, these

zones having a thinner brittle layer act like a car's crumple zone that cushions the impact during a collision.

The principle is rather simple. When shortening is applied, the part of the model that includes a "weak zone" at its extremities tends to move forward in a rigid fashion while being pushed by the moving end wall. The same applies to the other half of the model, but the movement is in the opposite sense (Fig. 3). This differential movement creates two separate blocks that slide one past each other, thereby generating a wrench zone between them. All of this is strictly independent of the underlying rigid basal plate as the viscous layer fully decouples the brittle layer from it.

Here, we present the two most informative experiments (named Model 1 and Model 2) to illustrate the processes and the most outstanding results. Note that for the sake of clarity, an arbitrary coordinate system has been assigned to the models as shown in Fig. 3 and it will be used for all overhead views and cross-sections in the rest of the manuscript.

3. Experimental results

In this section, we summarize the main experimental results according to the lateral confinement of the experiments during shortening in both confined and unconfined models.

3.1. Model 1: two moving end walls and model laterally confined

The first model (Model 1) was initially 112 cm long and 40 cm wide, with the "weak zones" located in the NE and SW corners of the sandbox, respectively (Fig. 4). Location of their edges were offset from the center of the model. The brittle overburden was laterally confined by the lateral glass sidewalls and both end walls moved towards the center of the model pushed by a motor-driven worm screw at a velocity of 5 mm/h (Fig. 4). The total displacement (shortening) of each moving end wall before the deposition of the syn-kinematic layer was 3 cm and at the end of the experiment 6 cm (12 cm of total shortening when both end walls displacement is combined).

The shortening transferred to the model by the movement of the two mobile end walls during early stages of the experiment pushed forward the brittle overburden without any apparent deformation on surface but with bulk layer-parallel shortening as a major component of deformation (Koyi et al., 2004). In contrast, the weak zones were preferentially shortened and uplifted. This triggered a right-lateral movement in the central part of the model and the development of a wrench zone (Fig. 5). In Fig. 5a, we highlighted three N–S passive markers (a, b, and c dashed white lines in Fig. 5a) on the overhead picture at the beginning of the model (without deformation) in order to illustrate the amount of strike-slip displacement and the deformation patterns between different parts of the model. As shortening started (Fig. 5b), two small oblique displacement, transpressional faults having an orientation similar to that of left-stepping Riedel R shears initiated from the corner of each weak zone and propagated along-strike towards the model's center (Fig. 5b and 6a). A set of partly overlapping WNW-ESE *en-échelon* R faults

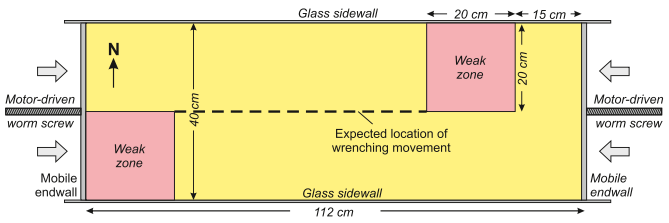

Fig. 4. Sketch of the experimental configuration of Model 1 (laterally confined system) at the top of the weak zones. Pink: viscous silicone. Yellow: brittle cover. (For interpretation of the references to color in this figure legend, the reader is referred to the Web version of this article.)

striking between 12° and 15° to the shortening direction develops in the northern sector of the model (Fig. 6a). In contrast, an E-W and WNW-ESE trending fault develop at the southern sector of the model (Fig. 6a). The differential displacement between both sets of faults develops a sigmoidal push up wide zone of dextral simple shear deformation that bends the squared passive grid on top of the model (Fig. 6a).

During ongoing shortening, deformation propagated further into the model as a wrench zone. Because the tips of the early-formed Riedel faults was laterally offset from each other, a restraining bend forms in the model's center that was subjected to transpression (Fig. 5c and 6b, and cross-section in Fig. 7). The deformed model shows three areas having different deformation patterns. Near the "weak zones" (in the areas of passive markers 1 and 3) wrenching of the brittle cover was accommodated by right-lateral Riedel R faults and synthetic shears in between, clearly visible on Fig. 6b. In contrast, in the central part of the model (Fig. 6a and b), the area located between markers 1 and 2 deformed by distributed strain with no clearly visible faults at surface (see the central part of the cross-section in Fig. 7), although two incipient faults, barely noticeable started to form (see black dashed lines in Fig. 6b).

After deposition of a syn-kinematic layer (Fig. 5d and 6c) increasing deformation caused the further propagation of the southern set of faults towards the opposite weak zone developing an anastomosing fault system formed by the linkage of R and P shears (Fig. 6c). In contrast, the propagation of the northern set of faults reach the central part of the model developing a fan of faults parallel to the shortening direction. An oblique anticline connects both fault systems (Fig. 6c). During the final stages of shortening, some incipient reverse faults developed on the N and NW flank of the anticline (Fig. 6c).

The N–S serial vertical cross-sections at the end of the experiment reveal how the thickening of the central area was accommodated by both the formation of a structural high (pop-up) and by subsidence into the viscous layer of the root of the thickened cover at depth (Fig. 7). So, most of the wrenching movement was accommodated in the brittle sand pack by distributed strain that thickened the entire unit (see little faulting in cross-sections of Fig. 7). The cross-sections show how the symmetry of the pop-up structure as well as its geometry changes along-strike (Fig. 7). The relief of the area with the oblique anticline is clearly asymmetric, with two clear vertical faults and a moderate dipping transpressional fault (Fig. 7a). This geometry rapidly changes along-strike to a thickened overburden with a symmetric relief (pop-up) on surface, and a root (pop-down) at depth (Fig. 7b and c). The thickness of the viscous layer decreases below the pop-down structure and increases in adjacent sectors indicating silicone flow during deformation.

3.2. Model 2: one moving end wall and model laterally unconfined

Model 2 was initially 112 cm long and 50 cm wide, and therefore, the width of the weak zones was also slightly larger (25 × 20 cm) (Fig. 8). The width was increased to keep the dimensions of the model domain the same as in model 1 to facilitate comparison, as the model 2 required inserting silicone trenches along the glass sidewalls. Unlike Model 1, deformation in Model 2 was applied by moving the eastern end wall at a velocity of 5 mm/h reaching a total displacement of 12 cm (Fig. 8 and movie in supplementary material). This displacement is the same as the sum of the total displacement of the two moving end walls in Model 1. As in Model 1, deformation created a differential movement along a wrench zone that separates two blocks that moved one past each other.

In Model 2 we slightly modified the set-up of Model 1 to reduce the confinement along the glass sidewalls (diminution of the N–S horizontal stress) (Fig. 8). This was achieved by vacuuming the brittle sand pack in two narrow trenches (5 cm wide) along the glass sidewalls (light blue rectangles in Fig. 8). Vacuuming creates a pressure head gradient above the horizontal silicone layer from the central part of the model, where the overburden is thicker and the pressure head higher, towards the trenches where there is no overburden resulting in minimal pressure

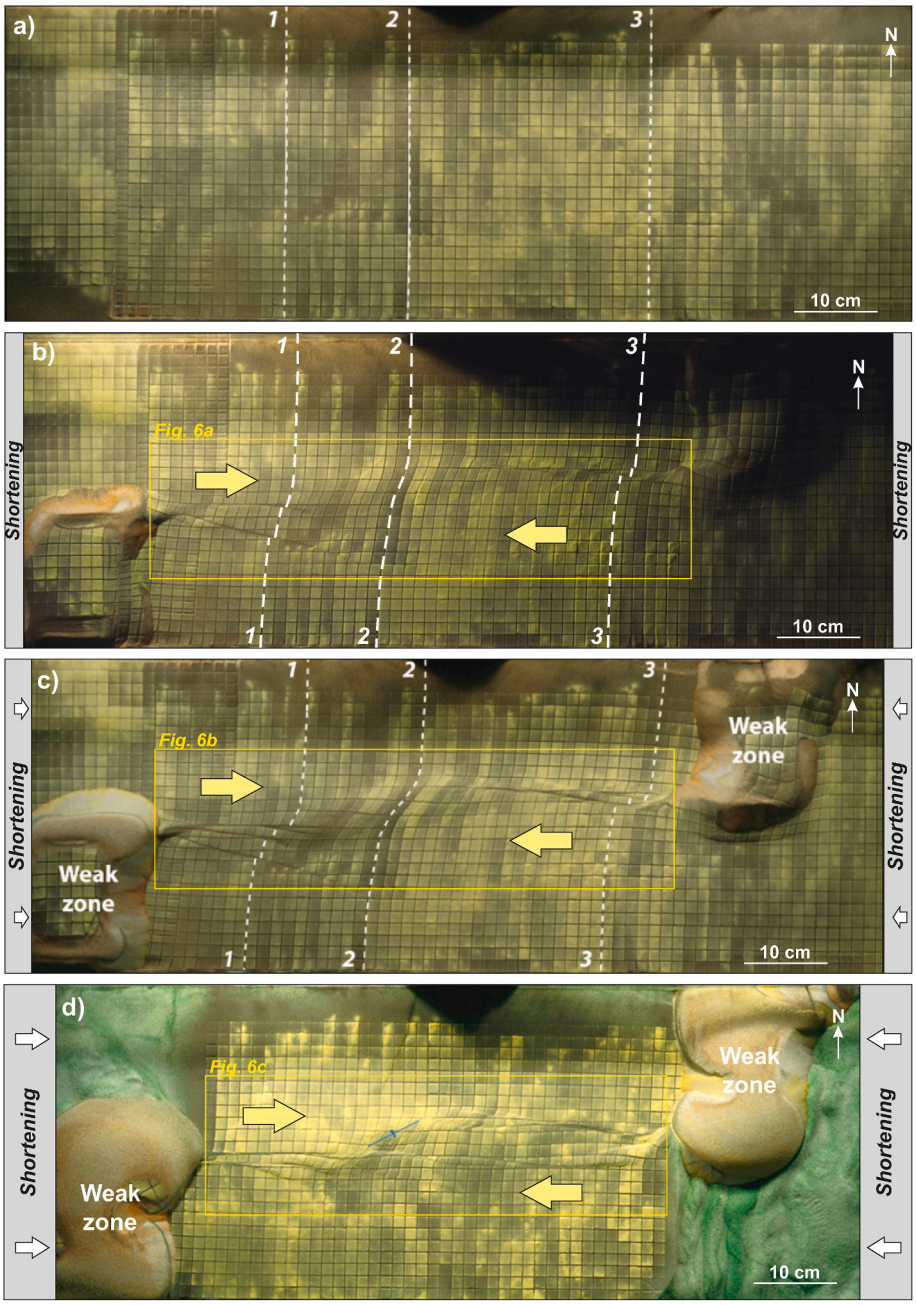

Fig. 5. Overhead photographs showing the evolution of Model 1. **a)** Beginning of the model; **b)** moderate shortening; **c)** severe shortening; and **d)** end of the experiment after deposition of a syn-kinematic green sand layer. White arrows inside the model: sense of relative displacement. White dashed lines and numbers 1, 2 and 3 are three initially N–S passive markers before (Fig. 5a) and during deformation (Fig. 5b and c). (For interpretation of the references to color in this figure legend, the reader is referred to the Web version of this article.)

head. The load variation triggers silicone flow along the pressure head gradient (Hudec and Jackson, 2007) adding a component of N–S extension. To reduce the impact of this pressure head gradient, and effectively minimize the lateral silicone flow, the trenches were promptly filled with silicone as in other works (e.g., Ferrer, 2012; Santolaria et al., 2015; Borderie et al., 2018). In this way, the lateral trenches acted as buffer zones along which the stress did not increase as much as in Model 1.

Once regional shortening begins, the deformation transferred to the brittle overburden preferentially deforms the weak zone closer to the moving end wall squeezing it and creating an E-W right-lateral wrench zone (Fig. 10a). Wrenching was initially accommodated by three partly overlapping *en-echelon* strike-slip faults trending slightly oblique to the shortening direction. These three faults quickly linked forming a unique fault that propagates along-strike towards the east as shortening increases (Fig. 10a). With increasing displacement, two new strike-slip faults initiate at locations that are slightly offset with respect to the tip of the pre-existing strike-slip fault and propagate towards the end walls until they reach the corner of the eastern and western weak zones (Fig. 10b). The linkage of these two new faults with portions of the previous ones results in a slightly curved major strike-slip zone connecting the two weak zones. The formation of this major structure also entails that the two ending splays of the first strike-slip fault progressively become inactive (Fig. 10c). After 5.5 cm shortening the slip of the major strike-slip fault continued throughout the experiment (Fig. 10c). At this point linkage of previous faults resulted in a narrow corridor with

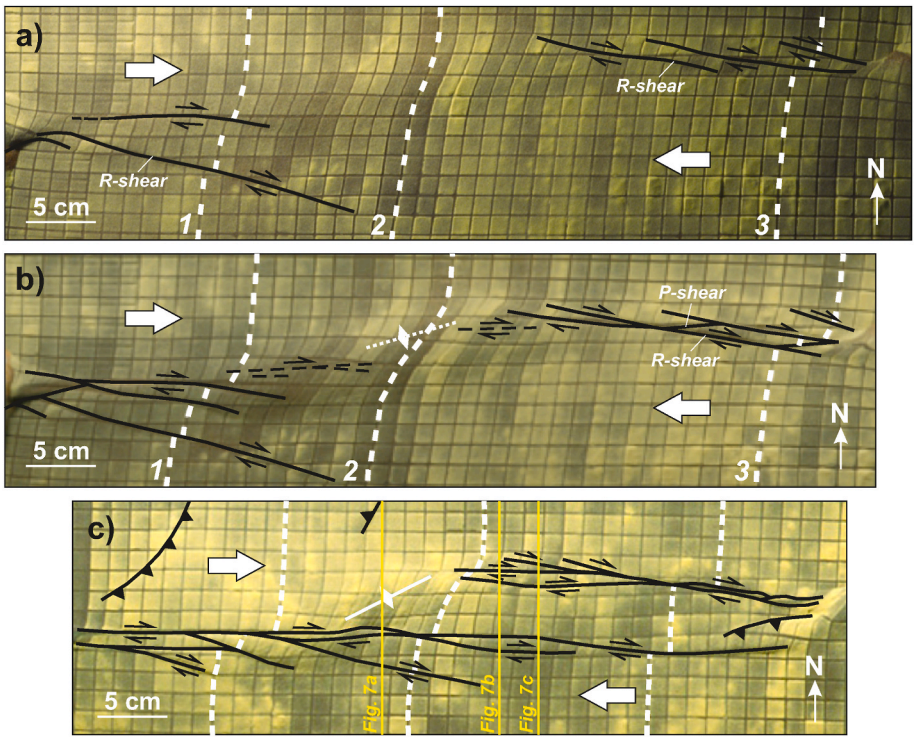

Fig. 6. Close-up interpreted photograph of the central part of the model 1 at the evolutionary stages of Fig. 5 (see specific locations in the yellow squares of this is figure). **a)** moderate shortening; **b)** severe shortening; and **c)** end of the experiment after deposition of a syn-kinematic layer with the location of the cross-sections of Fig. 7. White arrows inside the model indicate the sense of relative displacement. Moving wall is located at the right of the figure. White dashed lines and numbers 1, 2 and 3 are three initially N–S passive markers during deformation. Black lines: strike-slip faults; black dashed lines: incipient strike-slip faults, black lines with triangles: thrusts, and white line: anticline. (For interpretation of the references to color in this figure legend, the reader is referred to the Web version of this article.)

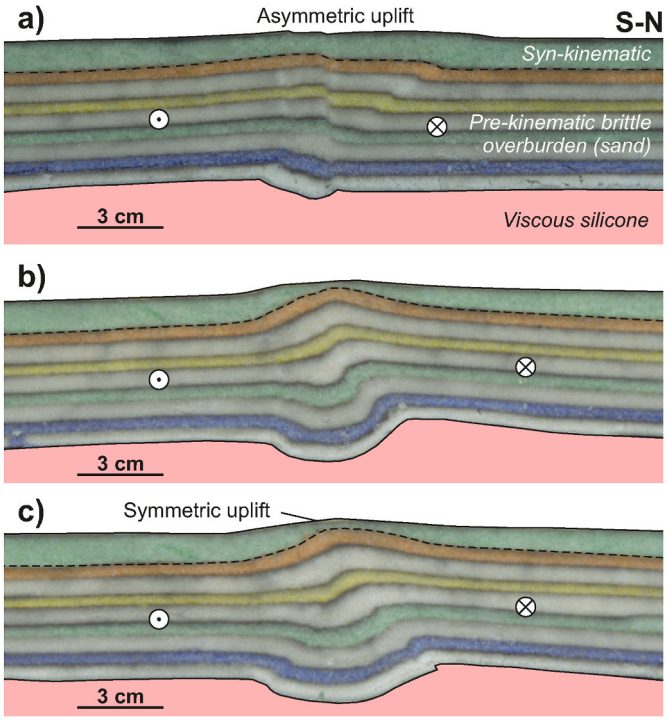

Fig. 7. Selected S–N vertical cross-sections at the end of Model 1 (location of the sections shown in Fig. 6c). The top green layer was deposited during a late stage of the experiment corresponding to the overhead view of Fig. 5d). Circle with a dot: motion into page; Circle with a cross: motion out of page. (For interpretation of the references to color in this figure legend, the reader is referred to the Web version of this article.)

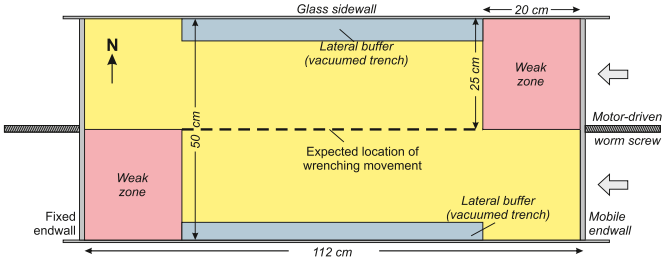

Fig. 8. Overhead view of the initial set up of Model 2. Red: viscous silicone. Yellow: brittle cover. Light blue: lateral buffer zones Sketch of the experimental configuration of Model 2 (laterally unconfined system) at the top of the weak zones. Pink: viscous silicone, yellow: brittle cover, blue squares: vacuumed lateral trenches to reduce confinement. (For interpretation of the references to color in this figure legend, the reader is referred to the Web version of this article.)

isolated lozenge blocks bounded by two steep strike-slip faults (Fig. 10c). A thrust perpendicular to the shortening direction develops on the brittle overburden near the mobile end wall (Fig. 9c). During mild shortening to the end of the model, two highly oblique strike-slip faults gradually propagate towards the southern edge of the major strike-slip zone (Fig. 10c). These faults that compartmentalize the southern sector of the model, progressively curve towards the strike-slip zone slightly displacing its southern strike-slip fault by several millimeters (Fig. 10c). At the end of the experiment an anastomosing wrench zone resulting from the linking of overlapped fault segments developed (Fig. 10c).

The narrowness of the central fault zone separating the two practically undeformed and horizontal sectors of the overburden is clearly illustrated by the cross section in Fig. 11. No significant vertical slip or

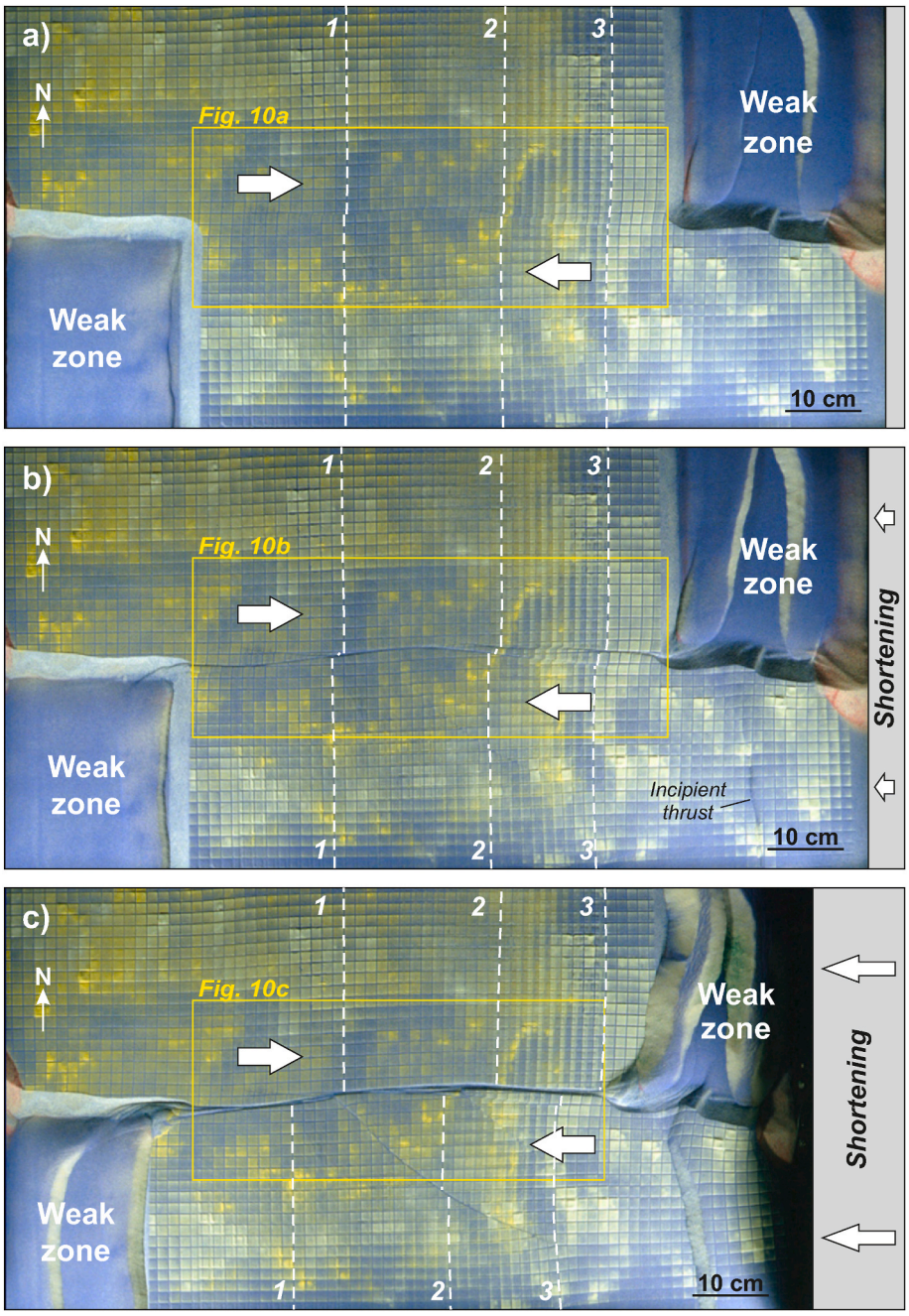

Fig. 9. Overhead photographs showing the evolution of Model 2. a) Beginning of shortening; b) mild shortening; and c) end of experiment after 12 cm shortening. White arrows inside the model: sense of relative displacement. White dashed lines and numbers 1, 2 and 3 are three initially N–S passive markers showing relative displacement during deformation. Black lines: faults; White dashed lines and numbers 1, 2 and 3) are three initially N–S passive markers before after deformation.

thickening occurred along the narrow fault zone.

Summarizing, Model 2 presents three major differences compared to Model 1. First, there was no transpression in the center (Figs. 9 and 10). Second, the wrench zone at the end of the experiment was made of one single corridor bounded by two razor-sharp, vertical strike-slip faults trending practically parallel with respect to the imposed direction of horizontal movement in the eastern sector of the model but slightly curved to the western one (Figs. 10 and 11). Third, the strike-slip fault did not initiate from the edges of the weak zones (Fig. 9a and 10a). Instead, it started to form in the model's center itself, then propagated both westward and eastward (compare Fig. 9a and b, and 10a and b).

4. Discussion

4.1. How the number of moving end walls affect the kinematic evolution of the models?

The two models presented in this work demonstrate that strike-slip deformation can be initiated without involving rigid basement plates with a velocity discontinuity in between. The use of a brittle-viscous model with weak zones in the brittle overburden is an effective way to nucleate and transfer strike-slip deformation.

Regional contraction was applied with two (Model 1) or just one (Model 2) moving end wall(s). As the appearance, sense and relative length of displacement vectors in both fault blocks indicate (compare

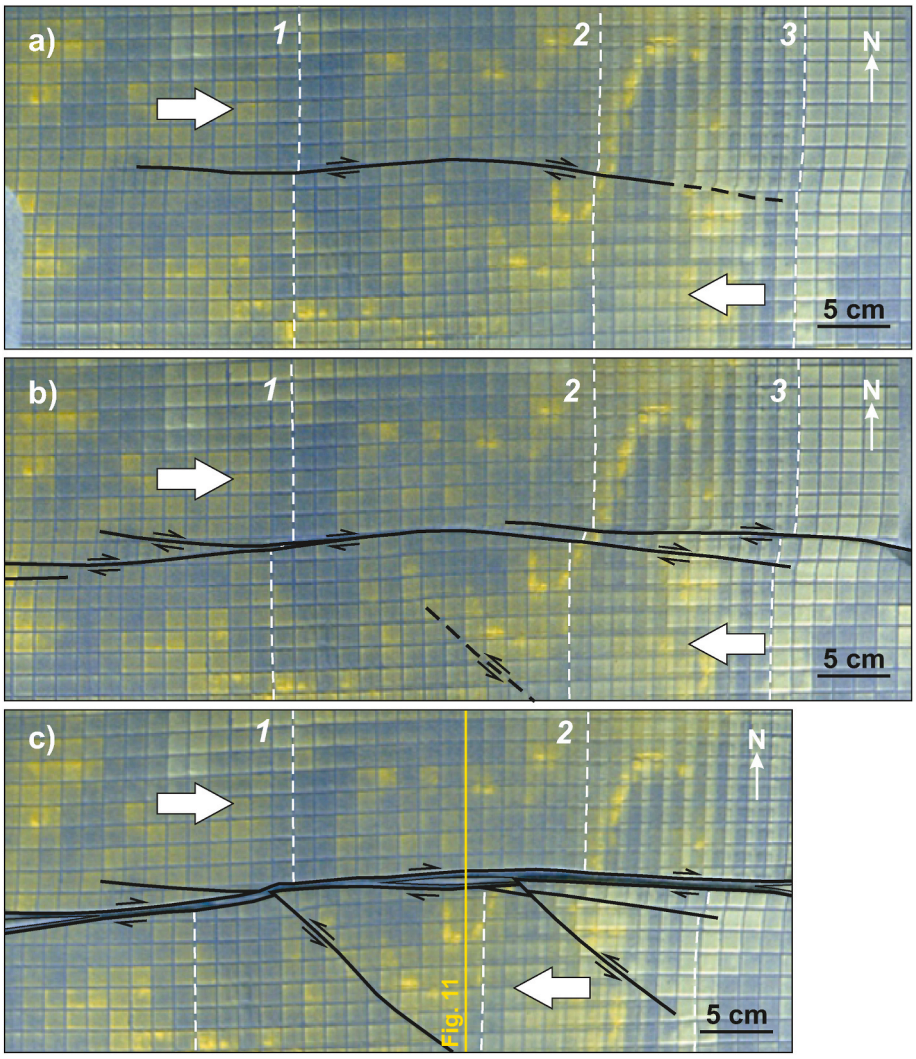

Fig. 10. Close-up interpreted photograph of the central part of the Model 2 at the evolutionary stages of Fig. 9 (see specific locations in the yellow squares of this is figure). **a)** Beginning of shortening; **b)** mild shortening; and **c)** end of the experiment with the location of the cross-sections of Fig. 11. White arrows inside the model indicate the sense of relative displacement. Moving wall is located at the right of the figure. White dashed lines and numbers 1, 2 and 3 are three initially N–S passive markers during deformation. Black lines: strike-slip faults; black dashed lines: incipient strike-slip faults. (For interpretation of the references to color in this figure legend, the reader is referred to the Web version of this article.)

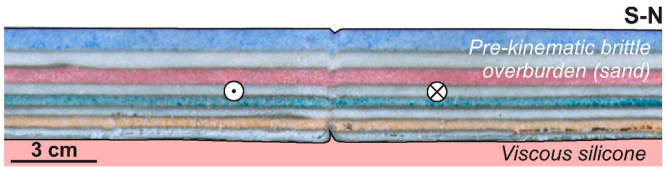

Fig. 11. S–N cross-section in the center of Model 2 (location of the section shown in Fig. 10c). To note the narrowness of the steeper wrench zone at the center of the picture.

displacement vectors between fault blocks in Model 1 and 2, Fig. 12a and b respectively), the number of walls through which shortening is transmitted into the model strongly affects the deformation pattern. During the early stages of Model 1 (two mobile end walls) contractional deformation is primarily absorbed by squeezing of both weak zones that uplifts and bulges the surface of the model above them (Fig. 5b). As shortening increases, the weak zones becomes completely uplifted above the pre-shortening regional relief by a thrust and backthrust (Fig. 5c). In contrast, in the equivalent sector where the model consists of sand, the initial component of deformation is layer-parallel shortening, but when the basal detachment of silicone becomes effective, the overburden is transported forward. In this part of the model, the length of the displacement vectors gradually decreases from the moving end wall towards the weak zones (Fig. 12a). The differential displacement between both sectors of Model 1 is accommodated by an oblique, transpressional fault with an orientation similar to that of Riedel shears (Fig. 6a). Wrench faults nucleated at the corner of each weak zone and propagated along-strike towards the center of the model (Fig. 6). Before the deposition of the syn-kinematic layer (Fig. 6b), two arrays of oblique faults linked by a large wrench fold (pop-up) resulted in a restraining bend with diffuse deformation that significantly thickened the overburden (Fig. 7). This is well illustrated by the total displacement vectors in the center of Model 1 (Fig. 12a), where the vectors with the shortest length are distributed following an ENE-WSW trend highlighting the transpressional component in the restraining bend.

On the other hand, just the weak zone adjacent to the mobile end wall in Model 2 is squeezed during the early stages of deformation with thrusts developing on the overlying sand cover (Fig. 9a). As shortening increases, this weak zone becomes narrower with greater displacement of the thrusts accommodating most of the contractional deformation (Fig. 9b). Like in Model 1, the initial deformation of the sector adjacent

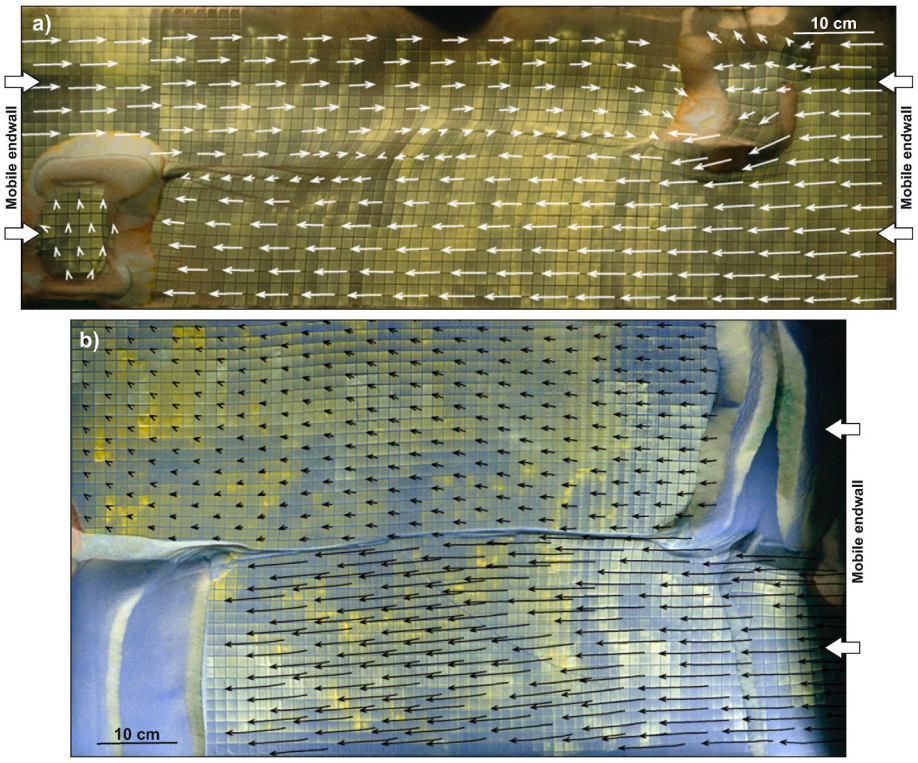

Fig. 12. Accumulated displacement vectors of Model 1 **(a)** and Model 2 **(b)** determined by measuring the location of the regular grid at the surface of the models during the deformation. Note how the length of the vectors is similar on both sides of the wrench zone in the model with two mobile end walls (Model 1, Fig. 12a), while in the model with a single mobile end wall (Model 2, Fig. 12b) they are much longer in the southern fragile sector displaced by the eastern mobile wall.

to the weak zone composed solely of sand is by layer-parallel shortening without any new relief. During mild shortening, a thrust trending parallel to the moving wall develops in the sector without a weak zone (Fig. 9b), and from this point outwards, the entire southern sector of the model is transported forwards over the silicone basal décollement (Fig. 9c). This results in the squeezing and thrusting of the weak zone located in the SW sector of the Model 2 (Fig. 9c). The displacement vectors of this model have all the same transport direction but show different lengths, being shorter in front of the weak zone where they gradually decrease towards the fixed end wall (Fig. 12b). The displacement difference between the northern and southern sectors of Model 2 is accommodated by an E-W right-lateral wrench zone in the central part of the model (Figs. 9 and 12b). However, the geometry and the structural style of the wrench zone is drastically different than the one of Model 1. In this case, the fault formed in the center of the model (Fig. 10a) and propagated along-strike very quickly towards the weak zones (Fig. 10b) to form an anastomosing strike-slip zone with overlaps and steps that remained active as horizontal shortening increases (Fig. 10c). The total displacement vectors highlight the sharp and clear boundary between the two fault blocks along the wrench zone without significant dip slip or thickening along the faults (Figs. 10 and 11), with strong different lengths at each fault block controlled by the experimental configuration with a single moving end wall (Fig. 12b).

4.2. *Effect of the lateral "buffer zones" on the orientation of Riedel faults*

The cause for the orientation of Riedel R faults in Model 1 is well known, as illustrated in Fig. 13a (Wilcox et al., 1973). During simple shear, the maximum principal stress, the σ_1 axis, is oriented at 45° from the direction of E-W imposed shear. With an angle of internal friction of

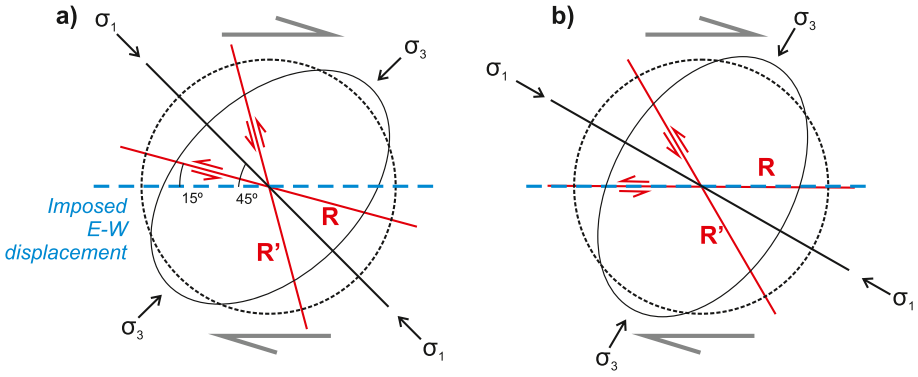

Fig. 13. a) Sketch illustrating the orientation of the maximum horizontal stress (σ_1) and the two potential Riedel faults (R and R′) in Model 1. **b)** Sketch illustrating how the orientation of the maximum horizontal stress (σ_1) can change when reducing the N–S horizontal stress (using lateral buffers in Model 2). Note that one of the two potential Riedel faults (R) is parallel to the direction of imposed movement (blue line). (For interpretation of the references to color in this figure legend, the reader is referred to the Web version of this article.)

about 30°, Riedel R faults form with an obliquity of about 15° with respect to the transport direction, thus leading to an *en-échelon* pattern between faults in the western and those in the eastern part of the model (Fig. 6a).

The change in orientation of the wrench zones in Model 2 is explained in Fig. 13b. Our hypothesis for such a change is that by lowering the N–S horizontal stress, the maximum principal stress was no longer oriented at 45° with respect to the transport direction (Model 1). The impact of having some lateral "buffer zones" lowers the horizontal stress, thereby changing the orientation of the maximum principal stress so that the Riedel R fault formed almost parallel with respect to the transport direction. Also note that during the latest stage (Figs. 9c and 10c), there was a slight component of movement towards the sidewalls resulting in the formation of Riedel R' faults in the southern sector of the model.

Similar structures have been described in salt-bearing rifted margin, where the downdip movement of salt due to gravity gliding caused by the margin tilting is significantly influenced by the geometry of the preexisting base salt relief. Dip-parallel or slightly oblique steps partition the deformation, forming strike-slip faults that separate domains of differential downslope translation (Dooley et al., 2017; Rowan, 2020). This type of structures is clearly illustrated in experiments conducted by Dooley et al. (2017). Figs. 4 and 7 of this work demonstrate that even when the roof blocks on either side of a presalt step are both moving downslope, the differential motions resulting from the base salt relief induce the development of Riedel shears that propagate from the basement step where the salt thickness increases. As in Model 2, this could validate the lack of confinement (N–S extension) as the primary control in this case.

In this way, the classical conceptual model is more realistic to study the deformation of a brittle overburden above a pre-existing strike-slip fault, while the new configuration is more realistic to study the initiation of wrench zones on a brittle cover fully decoupled from its basement by a ductile layer and without a pre-existing fault (i.e., salt-bearing basins).

4.3. Bruno Vendeville's legacy: modelling strike-slip deformation with no pre-imposed boundary conditions

The current models illustrate an alternative modelling set-up to reproduce strike-slip deformation designed by Bruno Vendeville in the late 90s. This experimental set-up reproduced strike-slip deformation, with no need to include motion of basal rigid plates and velocity discontinuity. This offers the system to respond freely to imposed boundary conditions avoiding the deformation localization effect of a basal VD, which would normally influence on the local stress orientation in a critical way (e.g., Morley, 1999).

In general, the laterally confined model, whose lateral boundary conditions resemble the classic Riedel experiments, show results in agreement to previous modelling works of this latter type (e.g., Cloos, 1928; Riedel, 1929; Tchalenko, 1970; Naylor et al., 1986). Wrenching is indeed accommodated by a broad zone combining folding and faulting, with the typical minor structures (e.g., R shears) and through-going transcurrent faults cutting the models and allowing the two halves to slip past each other. This supports the validity of the current set-up to model strike-slip deformation. This configuration represented a step forward with respect to the classic Riedel experiments and opened new experimental possibilities to simulate other scenarios with strike-slip deformation. This is the case of salt-bearing rifted margins where during gravity gliding or spreading the seaward movement of the overburden commonly varies between adjacent depocenters or between adjacent domains of depocenters locally causing relative strike-slip between units moving at different rates (Rowan, 2020). One of these linear left-lateral strike-slip fault parallel to the regional dip and rooted in the edge of a shallow salt sheet of the northern Gulf of Mexico is clearly illustrated in the time slice of F ig. 25 by Rowan et al. (1999). Other works based on analogue models also produced strike-slip tear faults linking shortened diapirs, salt walls or salt canopies (e.g., Rowan and Vendeville, 2006; Ferrer, 2012; Dooley et al., 2017, 2023; Duffy et al., 2018; Santolaria et al., 2021). The salt of the diapirs preferentially accommodates the shortening forcing the overburden, in places, to fragment into blocks with different shortening-parallel displacements reflecting the progressive development of strike-slip tear faults. The depth slice of F ig. 22a by Dooley et al. (2023) shows the system of faults and strike-slip tear faults linking the stems of several diapirs beneath a salt canopy.

The setup presented in this work may be better suited for analyzing the influence of lateral variations in rheology at different crustal and/or lithospheric scale on strike-slip deformation, an effect which may be masked by the use of a basal VD, which may otherwise affect the stress field an resulting structural pattern in a dominant way. Similarly, the effect on stress reorientation and structure development of pre-existing brittle (discrete or pervasive) fabrics may be masked by the use of basal rigid plates (e.g., Morley, 1999) and therefore the use of the set-up designed by Bruno Vendeville may be more efficient to simulate such effect. Varying the overlapping of weak zones and working in extensional or compressional scenarios, the presented set-up could be useful to generate releasing or restraining bends, respectively. In fact, with some additional modifications the set-up presented in this work has been used to model the spontaneous formation of pull-apart basins (Boussarsar et al., 2022; Peng et al., 2024). In the experimental configuration by Boussarsar et al. (2022), the weak zones located in front of the mobile end walls partially overlap, but in addition they vacuumed two trenches in the overburden that also overlap and did not force the location of wrench zones when shortening started (see Fig. 8 by Boussarsar et al., 2022 for more details). The area between the two wrench zones without any pre-existing structure evolved to a pull-apart basin as shortening increased. Furthermore, although it has not yet been modeled, the experimental configuration used by Boussarsar et al. (2022) and Peng et al. (2024) can be useful to simulate the rise or rejuvenation of salt structures in pull-apart basins.

In addition to present an alternative to Riedel experiments, the set-up designed by Bruno Vendeville uses silicone not only as a salt analogue but as a medium localizing the deformation. The weak zones made by silicone are mechanically weaker than the surrounding sand and preferentially localize contractional deformation. This allows the development of the E-W right-lateral wrench zone due to the differential displacement between both parts of the models as shortening progresses (Figs. 5 and 9). Other authors used different types of weak zones made by silicone to localize deformation in different geological scenarios. Le Calvez and Vendeville (2002) used for the first time silicone ridges on predetermined locations over a silicone layer to nucleate and propagate extensional faults along-strike into the overlaying brittle sand cover. Their set-up represented a revolution compared to the classic fragile models where extensional faults or relay zones between offset extensional faults were forced by a velocity discontinuity made by a basal plastic sheet or metal plate (e.g., McClay and Ellis, 1987). This practice was incorporated as a guideline in analogue modelling methodology and has been used in numerous works (e.g., Zwaan and Schreurs, 2017; Molnar et al., 2019; Zwaan et al., 2019, 2021 among others). Dooley and Schreurs (2012) used weak zones made by silicone over a silicone detachment covering two basal rigid plates that slide one past each other along a strike-slip basement fault. The weak bodies with different geometries (rectangular walls and cylinders) representing dykes or salt walls were located over the basement fault trace with different orientations and then covered by sand. Restraining or releasing stepovers developed depending on the weak zone's orientation respect the basement fault trace. Dooley and Hudec (2020) and Wilson et al. (2023) presented a series of models simulating segmented rift systems that were subsequently inverted. To avoid internal artifacts as the ones described in set-ups with a basal rubber sheet (e.g., Amilibia et al., 2005), these authors used silicone slabs of triangular and rectangular sections over a thin basal silicone layer which in turn covered the rubber sheet. In this

way, the movement of the moving end walls produced rubber sheet's stretching which was transferred to the silicone detachment deforming the slabs allowing the nucleation of extensional faults at their edges forming half-graben (triangular slabs) or graben (rectangular slabs).

5. Conclusions

We have presented an alternative experimental configuration to the classical Riedel experiment to trigger wrenching or regional strike-slip. The set-up demonstrates that initiating strike-slip does not necessarily require to be transmitted from the base up using a rigid basement with a velocity discontinuity simulating a pre-existing structural fabric or basal discontinuities as in Riedel experiments.

By using zones of weakness simulating sedimentary basins at crustal scale or dormant diapirs or salt massifs at smaller scale, strike-slip can occur spontaneously above a viscous layer under the influence of lateral shortening, rather than by the stresses imposed by traction of basal blocks.

Where lateral confinement is high (Model 1), the potential slip planes are oblique to the direction of imposed movement. Early individual R1s are short-lived as the fault zone with significant component of dip-slip evolves. Flower structures and wrench folds form and strata are thickened by lateral contraction.

Where lateral confinement is lower (using lateral buffers as in Model 2), there is little or no conflict between the direction of potential slip planes (controlled by the orientation of principal stresses) and that of the imposed regional displacement. Deformation can be accommodated by a simple, narrow and permanent, vertically-dipping strike-slip fault.

The degree of overlap between the weak zones opens up a new set of modelling possibilities in future works on extensional or compressional scenarios to generate releasing or restraining bends respectively, as well as to model the reactivation or rejuvenation of pre-existing salt structures in wrench tectonics.

CRediT authorship contribution statement

B.C. Vendeville: Writing – original draft, Supervision, Methodology, Investigation, Formal analysis, Conceptualization. **G. Corti:** Writing – review & editing, Writing – original draft, Validation, Formal analysis. **M. Boussarsar:** Writing – review & editing, Writing – original draft, Validation, Formal analysis. **O. Ferrer:** Writing – review & editing, Writing – original draft, Visualization, Formal analysis.

Declaration of competing interest

The authors declare that they have no known competing financial interests or personal relationships that could have appeared to influence the work reported in this paper.

Data availability

Data will be made available on request.

6. Acknowledgments

The experiments presented here were conducted by the first author with the contribution of Laurent Boniface, then student at the University of Perpignan Via Domitia, when Bruno Vendeville was working at the Applied Geodynamics Laboratory (AGL), Bureau of Economic Geology (BEG), The University of Texas at Austin. This work was, at that time, funded by a consortium of the following companies: Amerada Hess Corporation, BHP Petroleum (Americas), BP Amoco Exploration, Chevron Petroleum Technology Co., ENI – AGIP, Exxon Mobil, Marathon Oil Company, PanCanadian Petroleum, Petroleo Brasileiro, Phillips Petroleum Company, Shell Oil Company, Texaco Exploration and Production, TotalFina, Unocal - Spirit 76, and Vastar Resources. Research of OF was partially supported by the SABREM project (PID2020-117598 GB-1000) funded by MCIN/AEI/10.13039/501100011033, and the Grup de Recerca de Geodinàmica i Anàlisi de Conques (2021SRG076) supported by the Secretaria d'Universitats i Recerca of the Departament d'Economia i Coneixement of the Generalitat de Catalunya. Frank Zwaan and two anonymous reviewers, as well as Hemin Koyi (Gest Editor), Mark G. Rowan (Editor of the Special Issue), and Ian Alsop (Editor-in-chief of Journal of Structural Geology) are also thanked for the handling of the manuscript and their helpful reviews and comments. Lastly, we extend our sincere gratitude to our friend, colleague and mentor Bruno for his significant contributions to the fields of analogue modelling and salt tectonics, and for continually inspiring us.

Appendix A. Supplementary data

Supplementary data to this article can be found online at https://doi.org/10.1016/j.jsg.2024.105166.

References

Amilibia, A., McClay, K.R., Sabat, F., Muñoz, J.A., Roca, E., 2005. Analogue modelling of inverted oblique rift systems. Geol. Acta 3, 251–271. https://doi.org/10.1344/105.000001395.

Ben-Avraham, Z., Lyakhovsky, V., 1992. Faulting processes along the northern Dead Sea transform and the levant margin. Geology 20, 1139–1142. https://doi.org/10.1130/0091-7613(1992)020<1139:FPATND>2.3.CO;2.

Borderie, S., Graveleau, F., Witt, C., Vendeville, B.C., 2018. Impact of an interbedded viscous *décollement* on the structural and kinematic coupling in fold-and-thrust belts: insights from analogue modeling. Tectonophysics 722, 118–137. https://doi.org/10.1016/j.tecto.2017.10.019.

Boussarsar, M., Vendeville, B.C., Abbes, C., Hassine, M., Ferrer, O., 2022. Analogue modeling of the role of salt in the structuration of thin-skinned pull-apart basins: the case study of El Hamma basin, Central Tunisia. J. Struct. Geol. 161, 104634 https://doi.org/10.1016/j.jsg.2022.104634.

Casas, A.M., Gapais, D., Nalpas, T., Besnard, K., Román-Berdiel, T., 2001. Analogue models of transpressive systems. J. Struct. Geol. 23, 733–743. https://doi.org/10.1016/S0191-8141(00)00153-X.

Cloos, E., 1955. Experimental analysis of fracture pattern. Geol. Soc. Am. Bull. 66, 241–256. https://doi.org/10.1130/0016-7606(1955)66[241:EAOFP]2.0.CO;2.

Cloos, H., 1928. Experimente zur inneren Tecktonik. Centralblatt für Mineralogie 12, 609–621.

Cloos, H., 1950. Die ostafrikanischen gräben. Geol. Rundsch. 38 (1), 66–67. https://doi.org/10.1007/BF01766576.

Corti, G., Moratti, G., Sani, F., 2005. Relations between surface faulting and granite intrusions in analogue models of strike-slip. J. Struct. Geol. 27, 1547–1562. https://doi.org/10.1016/j.jsg.2005.05.011.

Dooley, T.P., Hudec, M.R., 2020. Extension and inversion of salt-bearing rift systems. Solid Earth 11, 1187–1204. https://doi.org/10.5194/se-11-1187-2020.

Dooley, T.P., Schreurs, G., 2012. Analogue modelling of intraplate strike-slip tectonics: a review and new experimental results. Tectonophysics 574–575, 1–71. https://doi.org/10.1016/j.tecto.2012.05.030.

Dooley, T.P., Jackson, M.P.A., Hudec, M.R., 2015. Breakout of squeezed stocks: dispersal of roof fragments, source of extrusive salt and interaction with regional thrust faults. Basin Reseach 27 (1), 3–25. https://doi.org/10.1111/bre.12056.

Dooley, T.P., Hudec, M.R., Carruthers, D., Jackson, M.P.A., Luo, G., 2017. The effects of base-salt relief on salt flow and suprasalt deformation patterns — Part 1: flow across simple steps in the base of salt. Interpretation 5 (1), SD1–SD23. https://doi.org/10.1190/INT-2016-0087.1.

Dooley, T.P., Jackson, M.P.A., Hudec, M.R., 2023. Growth and evolution of salt canopies on a salt-detached slope: insights from physical models. AAPG (Am. Assoc. Pet. Geol.) Bull. 107 (2), 2053–2089. https://doi.org/10.1306/08072222013.

Duffy, O.B., Dooley, T.P., Hudec, M.R., Jackson, M.P.A., Fernandez, N., Jackson, C.A.L., Soto, J.I., 2018. Structural evolution of salt-influenced fold-and-thrust belts—a synthesis and new insights from basins containing isolated salt diapirs. J. Struct. Geol. 114, 206–221. https://doi.org/10.1016/j.jsg.2018.06.024.

Duffy, O.B., Dooley, T.P., Hudec, M.R., Fernandez, N., Jackson, C.A.-L., Soto, J.I., 2021. Principles of shortening in salt basins containing isolated minibasins. Basin Res. 33 (3), 2089–2117. https://doi.org/10.1111/bre.12550.

Ferrer, O., 2012. Salt Tectonics in the Parentis Basin (Eastern Bay of Biscay): Origin and Kinematics of Salt Structures in a Hyperextended Margin Affected by Subsequent Contractional Deformation. Universitat de Barcelona, p. 322. Ph.D. thesis.

Ferrer, O., Roca, E., Vendeville, B.C., 2014. The role of salt layers in the hangingwall deformation of kinked-planar extensional faults: insights from 3D analogue models and comparison with the Parentis Basin. Tectonophysics 636, 338–350. https://doi.org/10.1016/j.tecto.2014.09.013.

Girdler, R.W., 1990. The Dead Sea transform fault system. Tectonophysics 180 (1), 1–13. https://doi.org/10.1016/0040-1951(90)90367-H.

Gomes, A.S., Rosas, F.M., Duarte, J.C., Schellart, W.P., Almeida, J., Tomás, R., Strak, V., 2019. Analogue modelling of brittle shear zone propagation across upper crustal

morpho-rheological heterogeneities. J. Struct. Geol. 126, 175–197. https://doi.org/10.1016/j.jsg.2019.06.004.
Hatem, A.E., Cooke, M.L., Toeneboehn, K., 2017. Strain localization and evolving kinematic efficiency of initiating strike-slip faults within wet kaolin experiments. J. Struct. Geol. 101, 96–108. https://doi.org/10.1016/j.jsg.2017.06.011.
Hubbert, M.K., 1937. Theory of scale models as applied to the study of geologic structures. Geological Society of American Bulletin 48, 1459–1520. https://doi.org/10.1130/GSAB-48-1459.
Hudec, M.R., Jackson, M.P.A., 2007. Terra infirma: understanding salt tectonics. Earth Sci. Rev. 82, 1–28. https://doi.org/10.1016/j.earscirev.2007.01.001.
Koyi, H.A., Sans, M., Teixell, A., Cotton, J., Zeyen, H., 2004. The significance of penetrative strain in the restoration of shortened layers—insights from sand models and the Spanish Pyrenees. In: McClay, K.R. (Ed.), Thrust Tectonics and Hydrocarbon Systems, vol. 82. AAPG Memoir, pp. 207–222.
Koyi, H., Ghasemi, A., Hessami, K., Dietl, C., 2008. The mechanical relationship between strike-slip faults and salt diapirs in the Zagros fold-thrust belt. J. Geol. Soc. 165 (6), 1031–1044. https://doi.org/10.1144/0016-76492007-142.
Le Calvez, J.H., Vendeville, B.C., 2002. Experimental designs to model along-strike fault interaction. In: Schellart, W., Passchier, C.W. (Eds.), Analogue Modelling of Large-Scale Tectonic Processes. Electronic Edition, Journal of the Virtual Explorer, the Virtual Explorer Pty. Ltd., Conder, Australia, pp. 1–17. https://doi.org/10.3809/jvirtex.2002.00043, 2002.
Letouzey, J., Sherkati, S., 2004. Salt movement, tectonic events, and structural style in the central Zagros fold and thrust belt (Iran). In: Salt Sediment Interactions and Hydrocarbon Prospectivity: Concepts, Applications, and Case Studies for the 21st Century: 24th Annual. Society of Economic Paleontologist and Mineralogists, pp. 753–778. https://doi.org/10.5724/gcs.04.24.0753.
Mandl, G., 1988. Mechanics of Tectonic Faulting: Models and Basic Concepts. Elsevier, p. 408.
McClay, K.R., Ellis, P.G., 1987. Analogue models of extensional fault geometries. In: Coward, M., Dewey, J., Hancock, P. (Eds.), Continental Extensional Tectonics, vol. 28. Geological Society Special Publication, pp. 109–125. https://doi.org/10.1144/GSL.SP.1987.028.01.09.
Molnar, N.E., Cruden, A.R., Betts, P.G., 2019. Interactions between propagating rifts and linear weaknesses in the lower crust. Geosphere 15, 1617–1640. https://doi.org/10.1130/GES02119.1.
Morley, C.K., 1999. How successful are analogue models in addressing the influence of pre-existing fabrics on rift structures? J. Struct. Geol. 21, 1267–1274. https://doi.org/10.1016/S0191-8141(99)00075-9.
Naylor, M.A., Mandl, G., Sijpesteijn, C.H.K., 1986. Fault geometries in basement induced wrench faulting under different initial stress states. J. Struct. Geol. 8, 737–752. https://doi.org/10.1016/0191-8141(86)90022-2.
Peng, Z., Graveleau, F., Vendeville, B.C., Wang, X., Averbuch, O., 2024. Interaction between basement inherited strike-slip structures and thrust wedge propagation in the northern Tianshan foreland basin: insight from analogue modelling experiments. J. Struct. Geol. 183, 105143 https://doi.org/10.1016/j.jsg.2024.105143.
Ramberg, H., 1981. Gravity, Deformation, and the Earth's Crust in Theory. Experiments and Geological Applications, second ed. Academic-Press, London, New York, p. 452. 978-0125768603.
Richard, P., Naylor, M.A., Koopman, A., 1995. Experimental models of strike-slip tectonics. Petrol. Geosci. 1, 71–80. https://doi.org/10.1144/petgeo.1.1.71.
Riedel, W., 1929. Zur mechanik geologischer brucherscheinungen. Centralblatt für Mineralogie. Geologie und Paläontologie B, 354–368. https://doi.org/10.1007/BF01803692.
Román-Berdiel, T., Gapais, D., Brun, J.P., 1997. Granite intrusion along strike-slip zones in experiment and nature. Am. J. Sci. 297, 651–678. https://doi.org/10.2475/ajs.297.6.651.
Rosas, F.M., Terrinha, P., Duarte, J., Baptista, L., Kullberg, C., Almeida, J., Almeida, P., 2014. Analog modelling of strike-slip fault (lateral) propagation from an elastic to a viscous medium: insights from trial experiments. Comunicações Geológicas 101 (3), 1429–1432.
Rowan, M.G., 2020. Chapter 11 - salt- and shale-detached gravity-driven failure of continental margins. In: Scarselli, N., Adam, J., Chiarella, D., Roberts, D.G., Bally, A. W. (Eds.), Regional Geology and Tectonics, second ed. Elsevier, pp. 205–234. https://doi.org/10.1016/B978-0-444-64134-2.00010-9.
Rowan, M.G., Vendeville, B.C., 2006. Foldbelts with early salt withdrawal and diapirism: physical model and examples from the northern Gulf of Mexico and the Flinders Ranges, Australia. Mar. Petrol. Geol. 23 (9–10), 871–891. https://doi.org/10.1016/j.marpetgeo.2006.08.003.
Rowan, M.G., Jackson, M.P.A., Trudgill, B.D., 1999. Salt-related fault families and fault welds in the Northern Gulf of Mexico. AAPG (Am. Assoc. Pet. Geol.) Bull. 83 (9), 1454–1484. https://doi.org/10.1306/E4FD41E3-1732-11D7-8645000102C1865D.
Santolaria, P., Vendeville, B.C., Graveleau, F., Soto, R., Casas-Sainz, A., 2015. Double evaporitic décollements: influence of pinch-out overlapping in experimental thrust wedges. J. Struct. Geol. 76, 35–51. https://doi.org/10.1016/j.jsg.2015.04.002.
Santolaria, P., Granado, P., Carrera, N., Schneider, C.L., Ferrer, O., Snidero, M., Strauss, P., Pelz, K., Roca, E., Muñoz, J.A., 2021. From downbuilding to contractional reactivation of salt-sediment systems: insights from analog modeling. Tectonophysics 819, 229078. https://doi.org/10.1016/j.tecto.2021.229078.
Schreurs, G., 1997. Experiments on faulting in zones of oblique shortening. Lead. Edge 16 (8), 1159–1163. https://doi.org/10.1190/1.1437756.
Schreurs, G., 2003. Fault development and interaction in distributed strike-slip shear zones: an experimental approach. In: Storti, F., Holdsworth, R.E., Salvini, F. (Eds.), Intraplate Strike-Slip Deformation Belts, vol. 210. Geological Society, London, Special Publications, pp. 35–52. https://doi.org/10.1144/GSL.SP.2003.210.01.03.
Schreurs, G., Colletta, B., 1998. Analogue modelling of faulting in zones of continental transpression and transtension. In: Holdsworth, R.E., Strachan, R.A., Dewey, J.F. (Eds.), Continental Transpressional and Transtensional Tectonics, vol. 135. Geological Society, London, Special Publications, pp. 59–79. https://doi.org/10.1144/GSL.SP.1998.135.01.05.
Schellart, W.P., Nieuwland, D.A., 2003. 3D evolution of a pop-up structure above a double basement strike-slip fault: some insights from analogue modelling. In: Nieuwland, D.A. (Ed.), New Insights into Structural Interpretation and Modelling, vol. 212. Geological Society, London, Special Publications, pp. 169–179. https://doi.org/10.1144/GSL.SP.2003.212.01.11.
Tchalenko, J.S., 1970. Similarities between Shear zones of different magnitudes. Geol. Soc. Am. Bull. 81, 1625–1640. https://doi.org/10.1130/0016-7606(1970)81[1625:SBSZOD]2.0.CO;2.
Toeneboehn, K., Cooke, M.L., Bemis, S.P., Fendick, A.M., Benowitz, J., 2018. Stereovision combined with particle tracking velocimetry reveals advection and uplift within a restraining bend simulating the Denali Fault. Front. Earth Sci. 6 https://doi.org/10.3389/feart.2018.00152, 10, Sec. Structural Geology and Tectonics.
Vendeville, B.C., Jackson, M.P.A., 1992. The rise of diapirs during thin-skinned extension. Mar. Petrol. Geol. 9, 331–353. https://doi.org/10.1016/0264-8172(92)90047-I.
Viola, G., Odonne, F., Mancktelow, N.S., 2004. Analogue modelling of reverse fault reactivation in strike-slip and transpressive regimes: application to the Giudicarie fault system, Italian Eastern Alps. J. Struct. Geol. 26 (3), 401–418. https://doi.org/10.1016/j.jsg.2003.08.014.
Weijermars, R., 1986. Flow behaviour and physical chemistry of bouncing putties and related polymers in view of tectonic laboratory applications. Tectonophysics 124, 325–358. https://doi.org/10.1016/0040-1951(86)90208-8.
Wilcox, R., Harding, T., Seely, D., 1973. Basic wrench tectonics. AAPG Bull. 57, 74–96. https://doi.org/10.1306/819A424A-16C5-11D7-8645000102C1865D.
Wilson, E.P., Granado, P., Santolaria, P., Ferrer, O., Muñoz, J.A., 2023. Inversion of accommodation zones in salt-bearing extensional systems: insights from analog modeling. Solid Earth 14, 709–739. https://doi.org/10.5194/se-14-709-2023.
Zwaan, F., Schreurs, G., 2017. How oblique extension and structural inheritance influence rift segment interaction: insights from 4D analog models. Interpretation 5, SD119–SD138. https://doi.org/10.1190/INT-2016-0063.1.
Zwaan, F., Schreurs, G., Buiter, S.J.H., 2019. A systematic comparison of experimental set-ups for modelling extensional tectonics. Solid Earth 10 (4), 1063–1097. https://doi.org/10.5194/se-10-1063-2019.
Zwaan, F., Chenin, P., Errat, D., Manastchal, G., Schreurs, G., 2021. Complex rift patterns, a result of interacting crustal and mantle weaknesses, or multiphase rifting? Insights from analogue models. Solid Earth 12, 1473–1495. https://doi.org/10.5194/se-12-1473-2021.